Chapter 13
Fluctuations and Dynamics of Magnetic Nanoparticles

Elena Vedmedenko and Michael Potthoff

Abstract The stability of magnetic moments in a nanostructure against thermal and quantum fluctuations and the real-time dynamics of strongly excited nanosystems on metallic surfaces are studied theoretically on the basis of microscopic models addressing the degrees of freedom on the atomic level. To this end, different theoretical approaches and computational tools are employed and developed, such as classical Monte-Carlo simulations, quantum-classical hybrid dynamics and time-dependent density-matrix renormalization group.

13.1 Introduction

Fluctuations and real-time dynamics of a magnetic moment in an infinite magnetic film, in an isolated nanostructure or in a nanostructure coupled to a nonmagnetic metallic surface can be very different from fluctuations of the spin degrees of freedom in a magnetic bulk system. In addition, the magnetic properties of real nanomagnetic samples are measured during a finite observation time [1]. This fact and the strong influence of the substrate electrons may give rise to a couple of sometimes rather fundamental questions. For magnetic nanoparticles and atomic clusters it also has considerable physical and technical consequences. Namely, the recent investigations on magnetic properties of nanoislands [2] very much rely on the fact that information, encoded in the magnetic state of a small unit representing a single bit, is sufficiently stable over the respective observation time. This stability is important for applications in magnetic data storage technology [3] and intimately related to the above-mentioned dynamical properties.

E. Vedmedenko (✉)
Institute of Nanostructure and Solid-State Physics, University of Hamburg, Hamburg, Germany
e-mail: vedmeden@physnet.uni-hamburg.de

M. Potthoff (✉)
I. Institute of Theoretical Physics, University of Hamburg, Hamburg, Germany
e-mail: michael.potthoff@physik.uni-hamburg.de

R. Wiesendanger (ed.), *Atomic- and Nanoscale Magnetism*, NanoScience and Technology, https://doi.org/10.1007/978-3-319-99558-8_13

The purpose of this review is threefold: (i) We first discuss, on a rather fundamental level, different theoretical approaches to the real-time dynamics of a single spin coupled to a metallic substrate or host. In particular, this discussion serves to place the famous Landau–Lifschitz–Gilbert (LLG) equation in a broader context. This is important as the LLG equation serves as the basis for extended and very successful simulations of dynamical properties of magnetic systems when formulated for several spins and when including various magnetic interactions and anisotropies.

(ii) In a second step, we move from dynamics to thermodynamics and consider the equilibrium thermal properties of a magnetic nanoparticle. In particular, we discuss the role of finite lateral dimensions of magnetic nanoobjects for the definition of various crossover and critical temperatures.

(iii) In the third part we finally address a couple of highlights of the application of the spin-dynamics theory and review the study of life-times of polarizations of magnetic adatoms placed on semiconducting and metallic substrates and perturbed by the tip of a spin-polarized scanning tunneling microscope (SP-STM) and discuss a theoretical proposal of the manipulation of magnetic domain walls by the SP-STM tip.

The chapter is organized as follows: Sect. 13.2 gives an introduction and some overview of the dynamics of spins coupled to conduction electrons. Spin dynamics in the prototypical Kondo-impurity model is discussed in Sect. 13.3, followed by linear-response theory in Sect. 13.4. Effects of electron correlations on the spin dynamics are addressed in Sect. 13.5. Section 13.6 is devoted to the theoretical description of static and dynamic correlation functions in nanomagnets of finite lateral extensions, while theoretical concepts of microscopic manipulation of magnetic domain walls at the nanoscale are reviewed in the last Sect. 13.7.

13.2 Dynamics of Spins Coupled to Conduction Electrons

The real-time dynamics of a classical spin $\boldsymbol{S}$ in an external magnetic field is determined by the Laudau–Lifschitz (LL) [4] equation

$$\dot{\boldsymbol{S}} = \boldsymbol{S} \times \boldsymbol{B} \,, \tag{13.1}$$

where we have absorbed constants, such as the $\boldsymbol{g}$-factor, Bohr's magneton μ_{B} and Planck's constant $\hbar$ in the definition of the field $\boldsymbol{B}$. Considering as a prototypical system a magnetic atom on a metallic surface, the LL equation does not realistically model the dynamics of the magnetic moment since there is a coupling to the substrate. This coupling will result in a damping of the spin dynamics. If, for example, the field direction is suddenly flipped from $-z$ to $+z$-direction, the spin will align to the new field direction, i.e., the system will reach its ground state in the course of time. This is well described by the Landau-Lifschitz-Gilbert (LLG) equation [4, 5],

$$\dot{\boldsymbol{S}} = \boldsymbol{S} \times \boldsymbol{B} - \alpha \boldsymbol{S} \times \dot{\boldsymbol{S}} \,, \tag{13.2}$$

where α is the famous Gilbert-damping constant.

There is a huge number of studies on spin-dynamics based on the LLG equation and of its various extensions [6, 7] covering many-spin systems, direct and indirect magnetic couplings between the spins, nonlocal Gilbert damping, and anisotropic interactions of different kind. Furthermore, the LLG approach is extremely successful in practice, even on an atomistic level [8]. On the other hand, from a fundamental perspective, the LLG equation (13.2) has been introduced phenomenologically. Apparently, it also violates energy and spin conservation. We will therefore consider a different theoretical route here and study the dynamics of a classical spin in contact with a large Fermi sea of conduction electrons by treating the electron degrees of freedom explicitly.

Figure 13.1 gives an overview: The paradigmatic model for a single spin coupled to a Fermi sea is the Kondo-impurity model. In case of a classical spin, the model is easily amenable to an exact numerical solution which is reminiscent of Ehrenfest dynamics in the context of molecular dynamics (see, e.g., [9] for an overview), where one also treats the nuclear degrees of freedom classically while the electron system is (effectively) noninteracting, i.e., moves in an effective single-electron potential. An important simplification is linear-response theory which applies to the weak-coupling limit. This approach is quite attractive since it represents a spin-only theory and, as the spin dynamics is typically much slower than the electron dynamics, allows us to access long time scales. The linear-response approach still keeps the full memory effects. This is not always necessary, and exploiting the largely different time scales of spins and electrons explicitly, one can re-derive the LLG theory with the help of a Markov approximation. The physics of the classical-spin Kondo model is very rich and has been studied in various ways and with various model extensions in recent years [10–13]. To some extent it will be reviewed here. Beyond that, there are quantum-spin effects, either on the exact level of the quantum-spin Kondo model or within a time-dependent hybridization mean-field theory [14], which become important for antiferromagnetic coupling, small spin quantum numbers and at extremely low temperatures. Below the Kondo temperature, time-dependent screening effects are worth being explored, see [12, 15, 16].

13.3 Tight-Binding Spin Dynamics

The prototypical model is the Kondo-impurity model of a classical spin coupled to a Fermi sea of conduction electrons:

$$H = \sum_{ij\sigma} T_{ij} c_{i\sigma}^{\dagger} c_{j\sigma} + J \boldsymbol{s}_{i_0} \boldsymbol{S} - \boldsymbol{B} \boldsymbol{S} \,. \tag{13.3}$$

The inset of Fig. 13.2 gives a sketch of the Hamiltonian. Here, a classical spin $\boldsymbol{S}$ with fixed length S is antiferromagnetically ($J > 0$) exchange-coupled to a system of conduction electrons hopping with an amplitude T_{ij} over the sites i, j of a lattice.

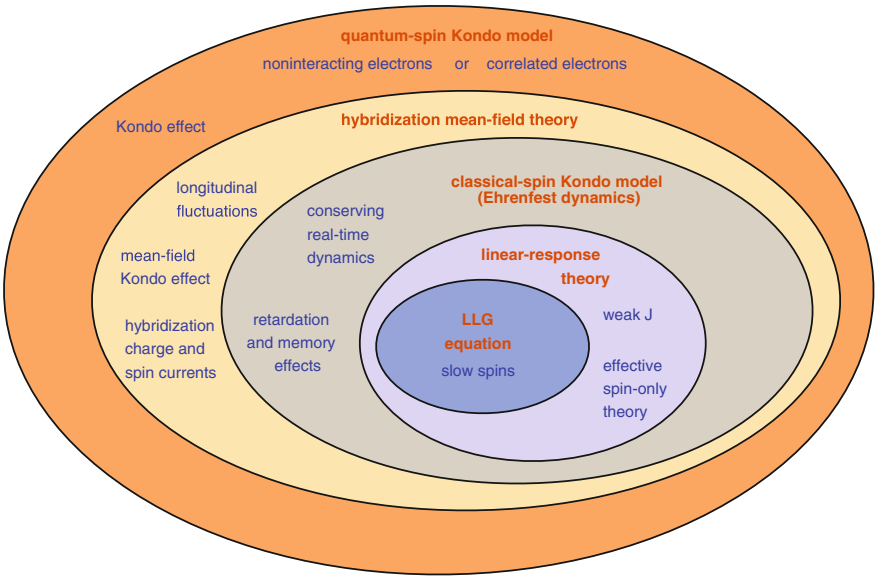

Fig. 13.1 Various approaches to real-time spin dynamics. See text for discussion

For simplicity, we assume $T_{ij} = -T$ for nearest neighbors on a one-dimensional chain of length L. Setting $T = 1$ fixes the energy and (with $\hbar \equiv 1$) the time scale. We further consider a half-filled system, i.e., if N is the total electron number, the electron density $n = \sum_{\sigma=\uparrow,\downarrow} \langle c^\dagger_{i\sigma} c_{i\sigma} \rangle$ is fixed to $n = N/L = 1$. Real-time dynamicsis initiated by suddenly flipping the field direction from $-z$ to z-direction at time $t = 0$, while the spin initially points in the $-z$-direction (with a slight distortion to break the symmetry).

We will start the discussion with the classical-spin Kondo (or s-d) model, i.e., with the numerically exact solution of the model (13.3). The equation of motion for $\boldsymbol{S}$ derives from the classical Hamilton function $H_{\text{class}} = \langle \Psi(t)|H|\Psi(t)\rangle$ and is of the LL form but with an additional Weiss field produced by the magnetic moment $\langle \boldsymbol{s}_{i_0} \rangle$ of conduction electrons at the site i_0 where the classical spin couples to. With the help of the Pauli matrices $\boldsymbol{\tau}$, this can be expressed in terms of the one-particle reduced density matrix $\rho = \langle c^\dagger c \rangle$ as $\langle \boldsymbol{s}_{i_0} \rangle = (1/2) \sum_{\sigma\sigma'} \rho_{i_0\sigma, i_0\sigma'} \boldsymbol{\tau}_{\sigma'\sigma}$. The equation of motion for ρ is of the von Neumann type and, besides the hopping matrix $\boldsymbol{T}$, involves a contribution from the Weiss field produced by $\boldsymbol{S}$. Therewith, one obtains a closed nonlinear system of coupled ordinary differential equations which can be solved by means of a high-order Runge-Kutta method, for example. System sizes of $L = 10^3$ are easily accessible in this way.

Figure 13.2 shows a typical result. After the sudden flip of the field, the x- and y-components of $\boldsymbol{S}$ show oscillations reflecting the precessional motion with Larmor frequency $\omega = B$. In addition, visible in the z-component, there is spin damping. The spin aligns to the new field direction in a few hundred inverse hoppings. This behavior

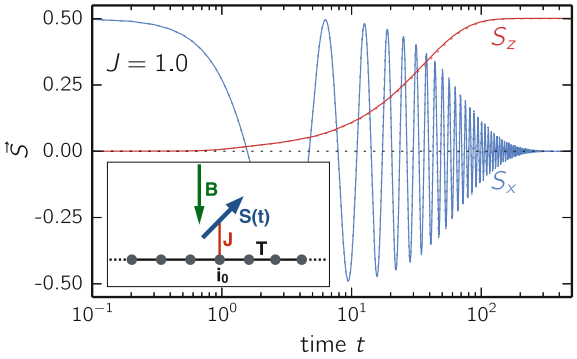

Fig. 13.2 (Adapted from [10]). Real-time dynamics of a classical spin (x and z components) within the model (13.3). Parameters: $S = 1$, $J = 1$, $L = 1001$, $i_0 = 501$, chain geometry with open boundaries. Energy and time units are chosen by fixing the nearest-neighbor hopping to $T = 1$. At time $t = 0$, the field direction is suddenly flipped from the $-z$ to the z direction. The inset provides a sketch of the system studied

is very much like the spin dynamics that could have been derived within the LLG framework, and one could easily extract a value of the Gilbert damping by fitting the numerical results. However, the spin dynamics shown in the figure emerges from a non-phenomenological, microscopic setup where, e.g., all macroscopic conservation laws resulting from the symmetries of H are fully satisfied. One should note that the energy of the local excitation of the system, $2BS$, is dissipated into the bulk such that *locally*, at i_0, the system approaches its ground state. The calculation stops at a maximum propagation time beyond which one would get (unphysical) distortions of the spin due to reflections from the open boundaries of the system. This also implies that the accessible time scale is approximately given by twice the half length of the chain divided by the Fermi velocity $v_F = 2T$. In our example, this amounts to about 500 inverse hoppings. Also the spin changes locally and thus, besides the energy, also spin must be transported into the bulk of the system. A detailed analysis [10] shows that this takes place in form of a spinful wave packet that is emitted from the core region, propagating with v_F and broadening slightly due to dispersion.

13.4 Linear-Response Theory

Typically, local exchange couplings are weak as compared to the energy scale set by the electron hopping and, therefore, a perturbative approach for the weak-J limit is reasonable (see "linear-response theory" in Fig. 13.1). Via standard time-dependent first-order perturbation theory in J, namely via the Kubo formula, $\langle \boldsymbol{s}_{i_0} \rangle_t = J \int_0^t dt' \chi_{\rm loc}(t - t') \boldsymbol{S}(t')$, the response of the conduction-electron magnetic moment at i_0 due to the spin that stirs in the Fermi sea can be expressed in terms of the local retarded magnetic susceptibility $\chi_{\rm loc}(t)$ at i_0. The latter is an equilibrium

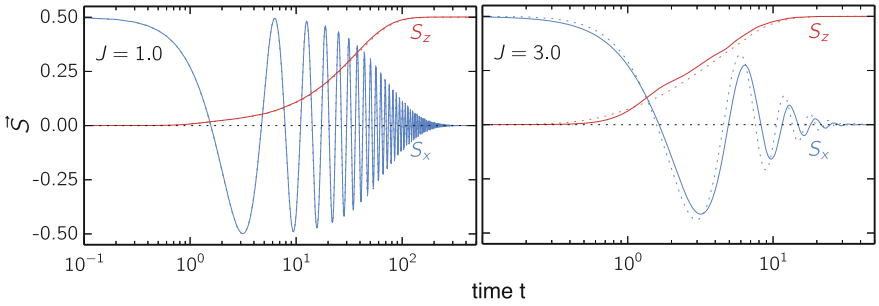

Fig. 13.3 (Adapted from [10]). Spin dynamics after a sudden flip of the field from x- to z-direction, as obtained by linear-response theory, see (13.4), for two different coupling constants J (solid lines). Dashed lines: results of the full tight-binding spin dynamics for comparison

quantity which can easily be calculated for a system of noninteracting electrons. Using this result for $\langle s_{i_0} \rangle_t$ the classical-spin equation of motion yields an effective spin-only theory, i.e., an equation of motion for an open quantum system with the full memory effect [10, 17, 18]:

$$\dot{\boldsymbol{S}}(t) = \boldsymbol{S}(t) \times \boldsymbol{B} - J^2 \boldsymbol{S}(t) \times \int_0^t dt' \chi_{\mathrm{loc}}(t - t') \boldsymbol{S}(t') \,. \tag{13.4}$$

Figure 13.3 shows corresponding results for $J = 1$ and $J = 3$. The linear-response theory provides extremely accurate results for rather strong couplings up to $J = 1$ as can be seen in the figure by comparing with the exact nonperturbative result, and only at $J = 3$ do we find significant deviations. This may appear surprising as the relevant dimensionless parameter tJ is not "small"; one should note, however, that its effects are rather moderate as only the non-adiabatic terms $\sim \boldsymbol{S}(t) \times \boldsymbol{S}(t')$ with $t \neq t'$ contribute, see (13.4). For $J = 3$ (see figure), visible artifacts of the linear-response theory already appear on a time scale which is smaller by almost two orders of magnitude as compared to the $J = 1$ case. This is attributed to the strong enhancement of retardation effects with increasing J, which lead to a much more effective perturbation.

The LLG equation (13.2) can be derived from (13.4) as a Redfield equation [19] using a Markov-type approximation [18, 20] which assumes that the electron dynamics is much faster than the spin dynamics. Formally, we exploit that the memory kernel $\chi_{\mathrm{loc}}(t - t')$ in (13.4) is peaked at $t' \approx t$ and cut the expansion $\boldsymbol{S}(t') \approx \boldsymbol{S}(t) + (t' - t)\dot{\boldsymbol{S}}(t) + \cdots$ at first order under the integral in (13.4). Furthermore, the upper bound of the integral must be set to infinity to get a constant. This is usually again justified by the peak structure of the kernel. With this we arrive at $\dot{\boldsymbol{S}}(t) = \boldsymbol{S}(t) \times \boldsymbol{B} - \alpha(t) \boldsymbol{S}(t) \times \dot{\boldsymbol{S}}(t)$ where the damping constant is given by

$$\alpha = -J^2 \int_0^\infty d\tau \, \tau \, \chi_{\mathrm{loc}}(\tau) \,. \tag{13.5}$$

Interestingly, for a one-dimensional system, this quantity is ill-defined as the integral diverges at the upper bound $t' \to \infty$ due to the slow long-time decay $\propto 1/t$ of the kernel (see [10] for a detailed discussion of this point). This implies that the LLG approach becomes questionable in one dimension. A pragmatic way out is to supplement the theory with an artificial cut-off for long times or by an *ad hoc* damping of van Hove singularities on the frequency axis. A physical regularization of the theory comes, for example, with the additional inclusion of electron-correlation effects.

13.5 Correlated Conduction Electrons

Electron correlations among the conduction electrons are expected to have a substantial impact on the spin dynamics. Within different models and using various approximations, this has been addressed in a few pioneering studies [21–23] but only via the effect of the Coulomb interaction on the Gilbert damping, i.e., in an indirect way. The emergence of new energy (and time) scales, however, is a hallmark of strongly correlated systems, and here the entire LLG concept is expected to break down. Studying these effects is important, e.g., for a microscopic understanding of the relaxation time scales emerging in modern nano-spintronics devices [24–26]. Here, we review our recent theoretical work [11] where the breakdown of the LLG theory is demonstrated by referring to the correlation-induced Mott insulator as a paradigmatic example [27].

We start from (13.4) assuming a weak (or moderate) coupling of the spin to the system of conduction electrons but replace the noninteracting Fermi sea by a one-dimensional Hubbard model with local Coulomb interaction U [28]. The time-dependent density-matrix renormalization-group approach (t-DMRG) [29–31] is used to compute the retarded local magnetic susceptibility of the Hubbard model, and the numerical solution of (13.4) provides us with the full memory and correlation effects. Results for different U are shown in Fig. 13.4.

At half-filling, the Hubbard model is a correlation-induced Mott insulator. For strong U, it perturbatively maps onto an antiferromagnetic Heisenberg model with Heisenberg coupling $J_{\mathrm{H}} = -4T^2/U$, i.e., there is a single energy scale only. Consequently, the susceptibility must show a scaling behavior according to $\chi_{\mathrm{loc}}(t) = F(tJ_{\mathrm{H}})$ with some function F. Inserting this into the expression for the Gilbert damping, (13.5), we find

$$\alpha = \frac{J^2}{J_{\mathrm{H}}^2} \int_0^\infty dx\, x\, F(x) = \frac{J^2}{J_{\mathrm{H}}^2}\alpha_0 = \frac{J^2U^2}{16T^4}\,\alpha_0\,, \tag{13.6}$$

where α_0 is a universal dimensionless Gilbert damping constant of a Mott insulator. From the numerical data we find $\alpha_0 \approx 4.8$. Thus, for fixed J, T, we have $\alpha \propto U^2$ implying that increasing interactions lead to a shorter spin relaxation time.

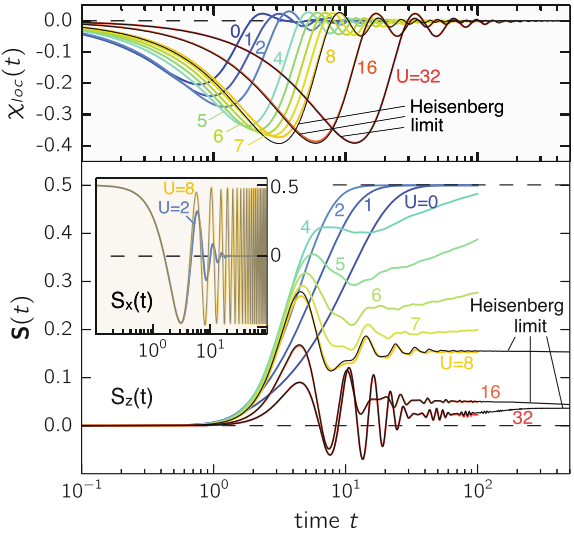

Fig. 13.4 (Adapted from [11]). *Upper panel:* Time dependence of the local spin susceptibility $\chi_{\rm loc}(t)$ at $i_0 = 1$ for an open Hubbard chain with $L = 60$ sites. t-DMRG for half-filling and different U as indicated. The nearest-neighbor hopping $T = 1$ fixes energy and time scales. *Lower panel:* Resulting real-time dynamics of a classical spin $\boldsymbol{S}(t)$ with $|\boldsymbol{S}(t)| = \frac{1}{2}$ coupled at $i_0 = 1$ (main plot: $S_z(t)$, inset $S_x(t)$). Calculations using (13.4) for $J = 1$ and different U. The spin dynamics is initiated by switching the field direction at $t = 0$ from x to z where $B_{\rm final} = 1$. Thin black lines: Heisenberg model with $J_{\rm H} = \frac{4T^2}{U}$ ($L = 400$) and, for improved accuracy at $U = 8$, with n.n. and n.n.n. couplings $J_{\rm H} = \frac{4T^2}{U} - \frac{16T^4}{U^3}$ and $J'_{\rm H} = \frac{4T^4}{U^3}$ [32] ($L = 300$)

The actual physics, however, is completely different: Fig. 13.4 (top panel) demonstrates that magnetic excitations which provide the dissipation of energy and spin to the bulk of the system get more and more weight with increasing U. However, they also become active on a later and later time scale. For $U \to \infty$ this means that they will actually never be activated and, since these magnetic excitations are the only ones available for a Mott insulator, this implies that there is no spin damping at all in this limit.

This expectation is indeed verified by the spin-dynamics results (see lower panel). In the weak-U regime, there is a fast relaxation of the spin to the field direction with a relaxation time which decreases with increasing U, see results for $U = 0$ up to $U = 2$. This regime is followed by some intermediate-coupling regime with a less regular behavior of $\boldsymbol{S}$. For an interaction strength of $U = 8$ or stronger, however, the relaxation time appears to diverge; the spin, after some initial dynamics, does not fully relax at all. It is easily shown, however, that a constant z-component of the spin and an undamped oscillation of the x- and y-component (see inset) is not a solution of the equation of motion (13.4). In the extreme long-time limit, we therefore expect that the spin finally undergoes a full relaxation.

The incomplete relaxation of the spin should be understood as a "pre-relaxation", i.e., analogously to the concept of prethermalization which is well known for purely electronic systems [33–36]. In cases of close parametric distance to points or limits of integrability, those systems are trapped, during a substantial period of time, in a prethermalized state and do not thermalize directly. For the present quantum-classical hybrid system and referring to relaxation rather than thermalization, the analog of the integrable point is given by the limit $U \to \infty$. Namely, for every finite time t, the memory kernel $\chi_{\rm loc}(t) \equiv 0$ in this limit, and thus (13.4) simplifies to the *linear* Landau-Lifschitz equation [4]. The situation is also similar to the case of quantum excitations which are metastable on a long time scale due to a very small phase space for decay. A prominent example is given by doublon excitations in the Hubbard model for interactions U much larger than the bandwidth [37–40]. Energy conservation requires the decay via a high-order process, such that the relaxation time diverges for $U \to \infty$.

13.6 Critical Properties and Magnetization Reversal in Nanosystems

Physical characteristics of the magnetization reversal are closely related to the critical properties of the object. While the critical properties of infinitely large magnets are well known, they have to be reconsidered for nanoparticles. One of the most important critical parameters is the Curie temperature. In the following, we describe some aspects of this critical temperature at the nanoscale and describe the magnetization switching in nanomagnetic ensembles.

13.6.1 Crossover Temperatures of Finite Magnets

From the experimental point of view, the critical temperature is a well defined quantity which can be measured. From the theoretical point of view, there is no Curie temperature as there is no phase transition in a system with a finite number of degrees of freedom and magnetic susceptibilities stay finite in the entire temperature regime. Nevertheless, they show enhancements at $T = T_{\rm C}(L)$, which defines a "reduced Curie temperature". Typically, one finds $T_{\rm C}(L) < T_{\rm C}(\infty)$ for open boundaries.

Above $T_{\rm C}(L)$, the magnetic state of the system is not stable temporally, but rather shows a superparamagnetic (SPM) behavior at temperatures $T_{\rm b}(L) < T < T_{\rm C}(L)$, which is neglected in finite-size scaling. For storage technology the blocking temperature $T_{\rm b}(L)$ is even more relevant than $T_{\rm C}(L)$ because it characterizes the crossover from the ferromagnetic (FM) state at low T to the SPM state, where the system changes its magnetization orientation between several energy minima determined by magnetic anisotropies. The $T_{\rm b}(L)$ is not a pure property of the system, but rather a

relative value, which depends on the observation time τ. For infinitely large τ, there is no temporal blocking of the magnetization because of quantum tunneling and thermal excitations, and thus $T_\mathrm{b}(L) \to 0$. For $\tau \to 0$ (referring to e.g. laser-probe methods), $T_\mathrm{b}(L) \to T_\mathrm{C}(L)$ while for intermediate τ (like in spin-polarized scanning tunneling microscopy) $0 < T_\mathrm{b}(L) < T_\mathrm{C}(L)$. This discussion shows that theoretical studies based on a microscopic spin model have to be refined when dealing with the superparamagnetic regime. A recent publication [41] shows that additional to a Monte-Carlo (MC) approach, where with an increasing number of MC steps per temperature, the blocking temperature $T_\mathrm{b}(L)$ decreases, a simple but reliable effective theory can cover the phenomenology of magnetic nanoparticles. A central quantity of this phenomenological theory is a two-point order-parameter correlation function defined between two spins $\mathbf{S}_i$ and $\mathbf{S}_j$ at sites $\mathbf{r}_i$ and $\mathbf{r}_j$ by

$$G(r) = \frac{1}{n(r)} \sum_{\substack{i<j \\ |r_i - r_j| = r}} \langle \mathbf{S}_i \mathbf{S}_j \rangle \,, \tag{13.7}$$

and a connected correlation function

$$\tilde{G}(r) = G(r) - M^2 = \frac{1}{n(r)} \sum_{\substack{i<j \\ |r_i - r_j| = r}} \left\langle S_i S_j \right\rangle - M^2 \,, \tag{13.8}$$

which explicitly takes account of the finite system size. Here, the sum in the first term runs over all $n(r)$ pairs separated by the distance r. The second term involves the magnetization $M = |\sum_i \langle S_i \rangle|/N$ with N being the number of sites. It turns out that the quantities defined above can be used for unambiguous definitions of $T_\mathrm{C}(L)$ and $T_\mathrm{b}(L)$, and moreover, lead to a new method to determine critical temperatures for infinite systems.

To get insight into the new method of determining the critical temperatures the above-defined correlation function $\tilde{G}(r)$ is evaluated and presented in Fig. 13.5 for a linear chain of Ising spins (see Fig. 13.5a) and for a 5×5 Ising system on a square lattice (Fig. 13.5b). Analyzing the data of Fig. 13.5 in detail we identify three specific temperatures: (i) For any finite T, the magnetization is $M = 0$, while for $T_1 = 0$ the magnetization jumps to $M = 1$. Therefore, the function $\tilde{G}(r)$ jumps from unity to zero as the temperature approaches $T = 0$ as seen in Fig. 13.5a, b. (ii) At the temperature T_2 ($1.7J$ in Fig. 13.5b) the curvature of $\tilde{G}(r)$ and $G(\mathbf{r})$ changes its sign. (iii) At the temperature $T_3 = 2.3J$ the trend of $\tilde{G}(r)$ changes from algebraic convex to exponential.

The first characteristic temperature T_1 is evidently equivalent to $T_\mathrm{b}(L)$. The mostly remarkable feature, however, is the change in the curvature of $\tilde{G}(r)$ from concave to convex at some temperature which cannot be expected from previously published results.

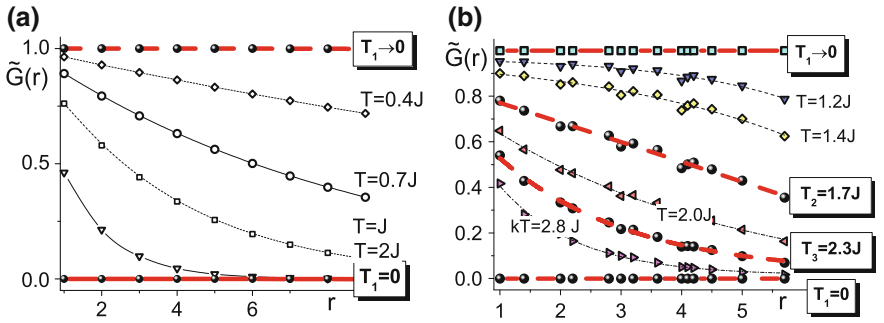

Fig. 13.5 (Adapted from [41]). **a** Two-point correlation functions $\tilde{G}(r)$ (symbols) calculated for an Ising chain with open ends and consisting of 10 atomic sites; **b** Two-point correlation functions for a 5×5 square lattice of Ising spins at $T = 0.5J \ll T_C(\infty)$. The lines in (**a**) and (**b**) are fits of the numerical data by the model correlation function given in (13.9). Three thick lines correspond to three critical temperatures: $T_b(L)$ - the blocking temperature, $T_C(L)$ the reduced Curie temperature, and $T_C(\infty)$ the Curie temperature of an infinite sample

To identify the physical meaning of T_2 and T_3, a model function $G(r)$ has been constructed.

$$G(r) = G(r, T) \approx B(T)e^{-r/\varepsilon(T)} + y(T)\,, \tag{13.9}$$

The form of $G(r)$ is reminiscent of the Ornstein-Zernicke theory. Note, however, that (13.9) refers to a finite system and that it applies to all distances r up to the system boundary. In particular, there are no constraints on the sign of the r-independent constants $\varepsilon(T)$, $B(T)$ and $y(T)$.

Using the above mentioned model, the numerically exact expectation values for the 1D, 2D and 3D finite Ising systems (Fig. 13.5) can be used to fit the parameters $\varepsilon(T)$, $B(T)$ and $y(T)$. It has been found that the quality of the fit is very good, see lines in (a) and (b) and it excellently describes the data in the entire temperature range. From this fit (see details in [41]) the temperature T_3 can be interpreted as the Curie temperature at a thermodynamic limit (infinite samples): $T_3 \approx T_C(\infty)$, and the temperature $T_2 = T_C(L)$ corresponding to the change in the curvature of $\tilde{G}(r)$ gives the reduced Curie temperature of a finite magnet. Thus, the described method yields a good estimate of $T_C(\infty)$, $T_C(L)$ and $T_b(L)$ from a single calculation without finite-size scaling. Analysis presented in [41] shows that $T_C(L)$ as well as $T_b(L)$ satisfy the finite-size scaling law $(T_C(\infty) - T(L))/T_C(\infty) = (L/L_0)^{-1/\nu}$ [42].

Hence, a simple analytical form for the two-point magnetic correlation function suggested in [41] for magnetic nanoparticles leads to an excellent numerical agreement with exact Ising, Heisenberg and Monte-Carlo data of finite anisotropic spin models and gives accurate definitions of crossover temperatures for finite systems.

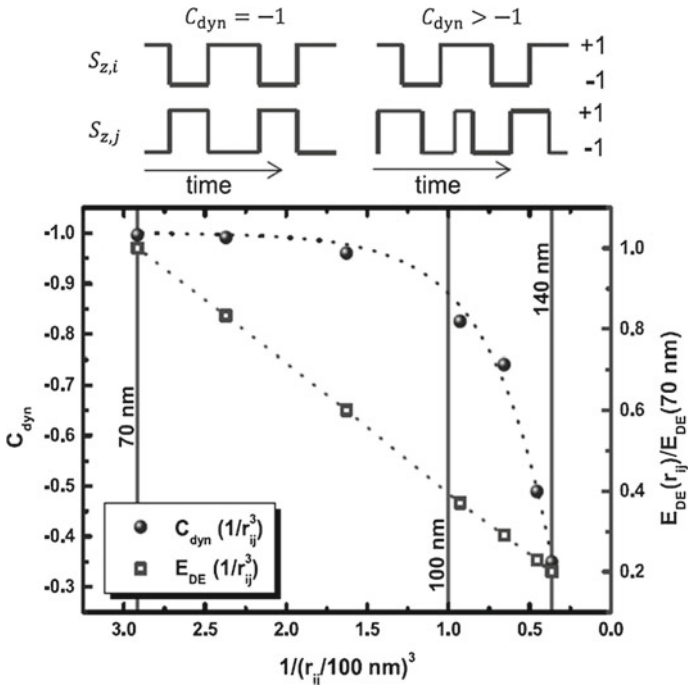

Fig. 13.6 Dynamical correlation-function C_{dyn} (spheres) and normalized dipolar energy C (circles) as a function of $1/r_{ij}^3$ normalized to 100 nm. It can be seen that C_{dyn} decreases more slowly than the C, which is responsible for the antiparallel correlation. The damping parameter $\alpha = 0.2$ has been considered in the calculations. The form of $C_{\mathrm{dyn}}(1/r_{ij}^3)$, however, is independent of α

13.6.2 Switching of Nanoparticles in Systems with Long-Range Interactions

While the described spin-spin correlations define averaged, time independent properties of nanosystems, the understanding of time-dependent correlations in nanomagnetic systems is also of great interest for fundamental science as well as for applications. Particularly crucial is the dynamical spin-spin correlation function for certain magnetic states used as bits of information, because the ultimate goal for any storage media is to create a highest possible packing density. This requires a small distance between islands or grains and, at the same time, one needs to switch the bits individually. So the question arises whether the spin-spin correlations remain the same in static (non-switching) and dynamical (switching) systems of identical geometry?

To investigate this exciting question theoretical and experimental investigations of magnetization reversal of ferromagnetic nanodots and their switching field distributions have recently been performed in [43–45]. In these investigations the dynam-

ical correlation function $C_{\mathrm{dyn}} = \int_{-\infty}^{\infty} dt\, S_{z,i}(t) S_{z,j}(t+s)$ between pairs of magnetic moments i and j has been considered. Hereby, S_z is the vertical component of moment i or j at times t and $t+s$, respectively. The proposed expression gives information on time correlations in a given state. For $C_{\mathrm{dyn}} \to 1$ the switching is correlated, while $C_{\mathrm{dyn}} \to 0$ corresponds to stochastic noise. The dynamical correlation function was calculated numerically for $s = 0$ and variable distances r_{ij} to check for the degree of correlation during the switching of different ensembles of dipolar nanoparticles coupled by the dipolar interaction [43]. The dependence of the correlation function on the interdot distance is shown in Fig. 13.6.

Figure 13.6 demonstrates that the time-dependent correlations decrease slower than the dipolar coupling itself. Even the dots at rather large separations ($r_{ij} > 140$ nm) show strong correlations (see Fig. 13.6), which are responsible for the in-phase switching of magnetization, although the dipolar energy is very weak at these large distances. The physical essence of this dynamical phenomenon is the time-averaged minimization of the potential energy of the ensemble of dots, which manifests itself in the many-body long-range correlations and prohibits dephasing of individual magnetic moments. Hence, the many-body dynamical effects described here, correspond to a minimization of a spin dynamical version of the action, rather than to a mere minimization of static dipolar energy. The most intriguing outcome of presented investigation is the long-ranged order of dynamical correlations and, thus, their influence on the collective states close to the thermal instability. The importance of these long-range order interactions and correlations for thermally assisted switching is supported by experiments described in [43].

13.7 Control of Ferro- and Antiferromagnetic Domain Walls with Spin Currents

There are two main concepts of the magnetic data storage: the first one relies on magnetic domains or other two-dimensional magnetic objects as bits of information; the second one uses one-dimensional transition regions between two domains; that is domain walls, as bits of information. Previous chapters were devoted to the switching of magnetic domains between two binary states corresponding to the first concept. Within the second concept towards new storage and logic devices the information is written or deleted by the current- and field-driven motion of magnetic domain walls (DWs) [46–48]. There are several proposals for reading or writing devices. Generally, an object corresponding to a bit of information has to be moved to the reading or writing device or the device has to be moved towards the bit. Nevertheless, it is difficult to address each DW individually in both cases, because a current often moves neighboring bits (DWs) in the same direction, whilst a magnetic field requires a movement in opposite directions. Domain walls can be individually addressed by the stray field coming from a tip of a magnetic force microscope (MFM) [49]. A particular challenge is, however, the manipulation of narrow DWs like those in monolayer thick

nanowires of Fe/W(111). The width of these walls is of the order of 2 nm, which is at least one order of magnitude smaller than the resolution of MFM. Therefore, new concepts for individual manipulations of such narrow DWs are required. One possible theoretical concept for such manipulations will be reviewed below [50–54].

In [50–52, 54] the manipulation of a magnetic DW was proposed to be performed by the tip of a Spin-Polarized Scanning Tunneling Microscope (SP-STM). The influence of an SP-STM tip on a DW has been studied by means of quantum- and classical atomistic spin dynamics as well as by Monte-Carlo (MC) simulations. Different modes, systems and time regimes were studied. The investigations have shown that this setup might be suitable for manipulation of ferromagnetic [50] as well as antiferromagnetic [51] domain walls. The theoretically proposed setup is depicted in Fig. 13.7.

An example is given by a ferromagnetic monolayer stripe of dimensions up to $L_x \times L_y = 40\,a \times 70\,a$ (15×26 nm (sc(001) or bcc(110) stacking) with the lattice constant a and classical Heisenberg moment $\mathbf{S_i} = (S_i{}^x, S_i{}^y, S_i{}^z)$ of unit length $\boldsymbol{\mu}_i/\mu_s$ at each lattice point. The magnetic properties are given by the following Hamiltonian:

$$\mathcal{H} = -J \sum_{\langle ij \rangle} \mathbf{S_i}\mathbf{S_j} - D_x \sum_i (S_i^x)^2 + D_z \sum_i (S_i^z)^2, \tag{13.10}$$

with $J > 0$ being the ferromagnetic exchange coupling between nearest neighbors, $D_x > 0$ an easy-axis and $D_z > 0$ a hard-axis anisotropy, respectively. The Heisenberg magnetic rotors were confined to the xy-plane by the anisotropies. The dipolar interaction of such an in-plane system is typically vanishing. Material parameters for Fe/W(110) or Co/Pt(111) monolayers ($J = 10...13$ meV, $D_x = 0...5$ meV and $D_z = 0...2.5$ meV) have been used in the calculations.

To describe the motion of DWs the generalized Landau-Lifshitz-Gilbert equation has been utilized:

$$\begin{aligned}\frac{\partial \mathbf{S}_i}{\partial t} = &- \frac{\gamma}{\left(1+\alpha^2\right)\mu_S}\mathbf{S}_i \times \left[\mathbf{H}_i + \alpha\left(\mathbf{S}_i \times \mathbf{H}_i\right)\right] \\ &+ \mathcal{C}\mathbf{S}_i \times \boldsymbol{\mathcal{T}}_i + \mathcal{D}\mathbf{S}_i \times \left(\mathbf{S}_i \times \boldsymbol{\mathcal{T}}_i\right)\ ,\end{aligned} \tag{13.11}$$

where γ is the gyromagnetic ratio, $\alpha = 0.025$ is the Gilbert damping, $\mathbf{H}_i = -\partial\mathcal{H}/\partial\mathbf{S}_i$ is the internal field, and $\boldsymbol{\mathcal{T}}_\mathbf{i}$ is the polarized spin current. The last two terms are the contributions corresponding to the precession and relaxation terms of the torque from the tunnel current. The concept similar to the case of a spin valve $\mathcal{C} = 0$ and $\mathcal{D} = 1$ has been used. In the numerical MC calculations, the sd-model has been used to account for the spin torque of tunneling electrons:

$$\mathcal{H}_\mathcal{T} = -\boldsymbol{g} \sum_i \boldsymbol{\mathcal{T}}_i \cdot \mathbf{S}_i, \tag{13.12}$$

with the coupling constant $\boldsymbol{g} = 1$. Here, the complete information on the current is provided by $\boldsymbol{\mathcal{T}}_\mathbf{i}$.

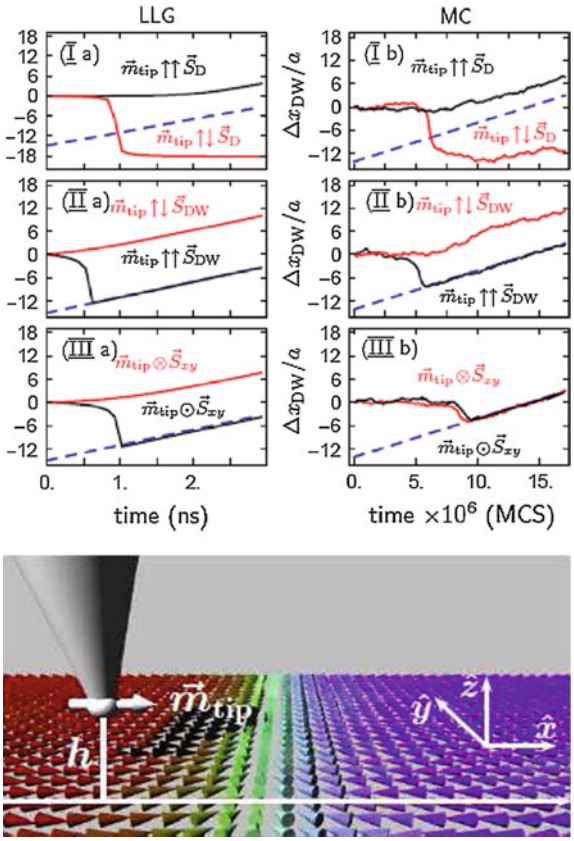

Fig. 13.7 Scheme of the initial state of the studied sample: two domains are separated by a DW elongated in y-direction, while the magnetic moments are pointing in $-x$ (blue) and $+x$ (red) directions. A tip with a magnetization $\boldsymbol{m}_{\text{tip}}$ and distance h from the sample moves towards the DW on the indicated track (white dashed line). Displacement of DW Δx_{DW} as a function of time obtained in MC simulations (left) and spin dynamics (LLG, right) are shown in the top panel. The tip moves with constant velocity marked by the dashed line. (I a) and (I b) correspond to a tip magnetization parallel and antiparallel to the initial domain ($\boldsymbol{m}_{\text{tip}} || \pm x$), (II a) and (II b) parallel and antiparallel to the DW orientation ($\boldsymbol{m}_{\text{tip}} || \pm y$), and (III a) and (III b) pointing into or out-of-plane ($\boldsymbol{m}_{\text{tip}} || \pm z$) [50]

The local strength and the orientation of the tunneling current can often be described by the Tersoff-Hamann model:

$$\mathcal{T}_{\mathbf{i}} = -I_0 \cdot \mathrm{e}^{-2\kappa\sqrt{(x_i - x_{\text{tip}})^2 + (y_i - y_{\text{tip}})^2 + h^2}} \cdot P \cdot \boldsymbol{m}_{\text{tip}}, \tag{13.13}$$

where P is the polarization of the SP-STM tip with magnetization $\boldsymbol{m}_{\text{tip}}$, κ is the inverse decay length of the wave function in vacuum, the time dependent tip and atom positions are $\mathbf{r}_{\text{tip}} = (x_{\text{tip}}, y_{\text{tip}}, h, t)$, $\mathbf{r}_i = (x_i, y_i, 0, t)$, and the current density

I_0. In the spin dynamics simulation we set $I_0 = 1.0 \cdot 10^7 \frac{\mu_S}{\gamma t J}$, However, the MC procedure does not allow for the direct time evaluation. Therefore, we choose a current density sufficiently high for domain wall manipulation. κ contains the work-function ϕ of the tip material and is set to 4.5 eV, in the range of magnetic materials used in experiments (e.g. Fe or Cr). For the chosen sample and tip parameters, we assume the spin torque acting on the magnetic moments to be large compared to Oersted-fields and Joule heating, which have been neglected in our simulations.

The following tip-sample geometries have been considered: (i) $\boldsymbol{m}_{\text{tip}} || \pm x$; (ii) $\boldsymbol{m}_{\text{tip}} || \pm y$, and (iii) $\boldsymbol{m}_{\text{tip}} || \pm z$. The explored initial set-ups are shown in Fig. 13.7. During the simulation, the tip is moved at a constant height $h \,||+ z$ along the stripe (in $+x$-direction) with a constant velocity v_{tip}. All presented calculations correspond to a constant height of the tip above the studied sample with a spin current, which is sufficiently high to influence the magnetization of a DW. The time dependence of the DW displacement Δx_{DW} for the three scenarios is plotted in Fig. 13.7. The black/gray solid curves correspond to the parallel/antiparallel orientation of the tip to a corresponding axis while the dashed line represents the tip displacement.

As one can see from Fig. 13.7 for ferromagnetic domain walls, almost all studied geometries are suited for DW manipulation as the black and gray lines corresponding to the displacement of the walls follow the dashed line representing the motion of the tip. One can also see that both simulation methods give identical results with one exception revealed for $\boldsymbol{m}_{\text{tip}} \otimes \mathbf{S}_{\text{d}}$. This effect is a result of the different simulation models and disappears in the regime of strong currents, when neglecting the hard-axis anisotropy, and also in the regime of strong damping. The detailed analysis given in [50–52] has demonstrated that there are at least three different modes suitable for DW manipulation, but the investigation of costs and benefits reveals the $\boldsymbol{m}_{\text{tip}} \uparrow\uparrow \mathbf{S}_{\text{DW}}$ as the optimal one. Similar calculations have been performed to study the possibility of manipulation of antiferromagnetic domain walls, which possess zero net magnetization. It has been concluded in [51, 52] that in order to manipulate such domain walls, the $\boldsymbol{m}_{\text{tip}}$ has to be othogonal to the magnetization of the domain as well as the domain walls. The directionality of the domain wall motion is identical for $\boldsymbol{m}_{\text{tip}} || \pm z$. To change the direction of the domain wall motion one has to change the orientation of the tip polarization to the opposite one [51, 52].

13.8 Conclusions

On the fundamental level, the studies that have been reviewed here can be extended in various ways: Most interesting is the generalization of the theory to the case of the Kondo lattice model, i.e., to several spins which represent, for example, a chain of magnetic atoms on a metallic surface. The real-time dynamics of such magnetic chains is crucially determined by the underlying electronic system, and there is not much known about such setups on the theoretical side. While long-time dynamics in the quantum-spin Kondo lattice is probably out of reach with the presently available numerical methods (also including the one-dimensional case), studying the classical-

spin Kondo lattice appears quite promising and first computations are in progress. Particularly, two-dimensional systems featuring the Kosterlitz-Thouless transition, systems with superconducting substrates (modeled by extensions of standard BCS theory to the inhomogeneous and time-dependent case) and systems in the extreme adiabatic limit, where the electron dynamics can be assumed to follow instantaneously the trajectories of classical spin configurations, represent highly interesting avenues for future research in this field. On the level of applications, the developed methods can be extended to describe the non-equilibrium dynamics of systems with complex magnetic structures and magnetic quasiparticles for their successful manipulation.

Acknowledgements We would like to thank David Altwein, Mario Krizanac, Roman Rausch, Mohammad Sayad, Thim Stapelfeldt, Kolja Them, Robert Wieser for the intense and fruitful cooperation over the years. Financial support of this work by the Deutsche Forschungsgemeinschaft through the Sonderforschungsbereich 668 (project B3) is gratefully acknowledged.

References

1. K. Binder, Rep. Prog. Phys. **60**, 487 (1997)
2. S. Krause, G. Herzog, T. Stapelfeldt, L. Berbil-Baitusta, M. Bode, E.Y. Vedmedenko, R. Wiesendanger, Phys. Rev. Lett. **103**, 127202 (2009)
3. E. Tsymbal, I. Zutic (eds.), *Handbook of Spin Transport and Magnetism* (Chapman and Hall/CRC, Florida, 2011)
4. L.D. Landau, E.M. Lifshitz, Physik. Zeits. Sowjetunion **8**, 153 (1935)
5. T. Gilbert, Phys. Rev. **100**, 1243 (1955); T. Gilbert, Magnetics, IEEE Trans. **40**, 3443 (2004)
6. G. Tatara, H. Kohno, J. Shibata, Phys. Rep. **468**, 213 (2008)
7. G. Bertotti, I.D. Mayergoyz, C. Serpico, *Nonlinear Magnetization Dynamics in Nanosystemes* (Elsevier, Amsterdam, 2009)
8. B. Skubic, J. Hellsvik, L. Nordström, O. Eriksson, J. Phys.: Condens. Matter **20**, 315203 (2008)
9. D. Marx, J. Hutter, Ab initio molecular dynamics: theory and implementation,in *Modern Methods and Algorithms of Quantum Chemistry*. NIC Series, Vol. 1, Ed. by J. Grotendorst, p. 301 (John von Neumann Institute for Computing, Jülich, 2000)
10. M. Sayad, M. Potthoff, New J. Phys. **17**, 113058 (2015)
11. M. Sayad, R. Rausch, M. Potthoff, Phys. Rev. Lett. **117**, 127201 (2016)
12. M. Sayad, R. Rausch, M. Potthoff, Europhys. Lett. **116**, 17001 (2016)
13. C. Stahl, M. Potthoff, Phys. Rev. Lett. **119**, 227203 (2017).
14. M. Sayad, L.M. Woelk, R. Rausch, M. Potthoff, unpublished (2017)
15. M. Medvedyeva, A. Hoffmann, S. Kehrein, Phys. Rev. B **88**, 094306 (2013)
16. M. Nuss, M. Ganahl, E. Arrigoni, W. von der Linden, H.G. Evertz, Phys. Rev. B **91**, 085127 (2015)
17. A. Sakuma, J. Phys. Soc. Jpn. **81**, 084701 (2012)
18. S. Bhattacharjee, L. Nordström, J. Fransson, Phys. Rev. Lett. **108**, 057204 (2012)
19. H.P. Breuer, F. Petruccione, *The Theory of Open Quantum Systems* (Oxford University Press, New York, 2002)
20. J. Fransson, Nanotechnology **19**, 285714 (2008)
21. E.M. Hankiewicz, G. Vignale, Y. Tserkovnyak, Phys. Rev. B **78**, 020404(R) (2008)
22. I. Garate, A. MacDonald, Phys. Rev. B **79**, 064404 (2009)
23. K.M.D. Hals, K. Flensberg, M.S. Rudner, Phys. Rev. B **92**, 094403 (2015)
24. M. Morgenstern, Science **329**, 1609 (2010)

25. S. Loth, M. Etzkorn, C.P. Lutz, D.M. Eigler, A.J. Heinrich, Science **329**, 1628 (2010)
26. A.A. Khajetoorians, J. Wiebe, B. Chilian, R. Wiesendanger, Science **332**, 1062 (2011)
27. F. Gebhard, *The Mott Metal-Insulator Transition* (Springer, Berlin, 1997)
28. J. Hubbard, Proc. R. Soc. Lond. A **276**, 238 (1963)
29. U. Schollwöck, Ann. Phys. (N.Y.) **326**, 96 (2011)
30. J. Haegeman, J.I. Cirac, T.J. Osborne, I. Pižorn, H. Verschelde, F. Verstraete, Phys. Rev. Lett. **107**, 070601 (2011)
31. J. Haegeman, C. Lubich, I. Oseledets, B. Vandereycken, F. Verstraete, Phys. Rev. B **94**, 165116 (2016)
32. L.N. Buleavskiĭ, Sov. J. Exp. Theor. Phys. **24**, 154 (1967)
33. M. Moeckel, S. Kehrein, Phys. Rev. Lett. **100**, 175702 (2008)
34. M. Moeckel, S. Kehrein, New J. Phys. **12**, 055016 (2010)
35. M. Kollar, F.A. Wolf, M. Eckstein, Phys. Rev. B **84**, 054304 (2011)
36. M. Marcuzzi, J. Marino, A. Gambassi, A. Silva, Phys. Rev. Lett. **111**, 197203 (2013)
37. A. Rosch, D. Rasch, B. Binz, M. Vojta, Phys. Rev. Lett. **101**, 265301 (2008)
38. N. Strohmaier, D. Greif, R. Jördens, L. Tarruell, H. Moritz, T. Esslinger, Phys. Rev. Lett. **104**, 080401 (2010)
39. F. Hofmann, M. Potthoff, Phys. Rev. B **85**, 205127 (2012)
40. R. Rausch, M. Potthoff, New J. Phys. **18**, 023033 (2016)
41. E. Vedmedenko, N. Mikuszeit, T. Stapelfeldt, R. Wieser, A.L.M. Potthoff, R. Wiesendanger, Eur. Phys. J. B **80**, 331 (2011)
42. O. Iglesias, A. Labarta, Phys. Rev. B **63**, 184416 (2001)
43. A. Neumann, D. Altwein, C.T. En, R. Wieser, A. Berger, A. Meyer, E.Y. Vedmedenko, H.P. Oepen, New J. Phys. **16**, 083012 (2014)
44. M. Krizanac, E.Y. Vedmedenko, R. Wiesendanger, New J. Phys. **18**, 033029 (2016)
45. M. Krizanac, E.Y. Vedmedenko, R. Wiesendanger, New J. Phys. **19**, 013032 (2017)
46. M.K. et al., J. Magn. Magn. Mater. **14**, 53 (2009)
47. R. Wieser, E.Y. Vedmedenko, R. Wiesendanger, Phys. Rev. B **79**, 144412 (2009)
48. R. Wieser, E.Y. Vedmedenko, P. Weinberger, R. Wiesendanger, Phys. Rev. B **82**, 144430 (2010)
49. T. Yamaoka, K. Watanabe, Y. Shirakawabe, K. Chinone, E. Saitoh, H. Miyajima, Jpn. J. Appl. Phys. **45**, 2230 (2006)
50. T. Stapelfeldt, R. Wieser, E.Y. Vedmedenko, R. Wiesendanger, Phys. Rev. Lett. **107**, 027203 (2011)
51. R. Wieser, E.Y. Vedmedenko, R. Wiesendanger, Phys. Rev. Lett. **106**, 067204 (2011)
52. R. Wieser, T. Stapelfeldt, E.Y. Vedmedenko, R. Wiesendanger, Eur. Phys. Lett. **97**, 17009 (2012)
53. P. Weinberger, E.Y. Vedmedenko, R. Wieser, R. Wiesendanger, Philoso. Magn. **91**, 2248 (2011)
54. K. Them, E.Y. Vedmedenko, K. Fredenhagen, R. Wiesendanger, J. Phys. A: Math. Theor. **48**, 075301 (2014)